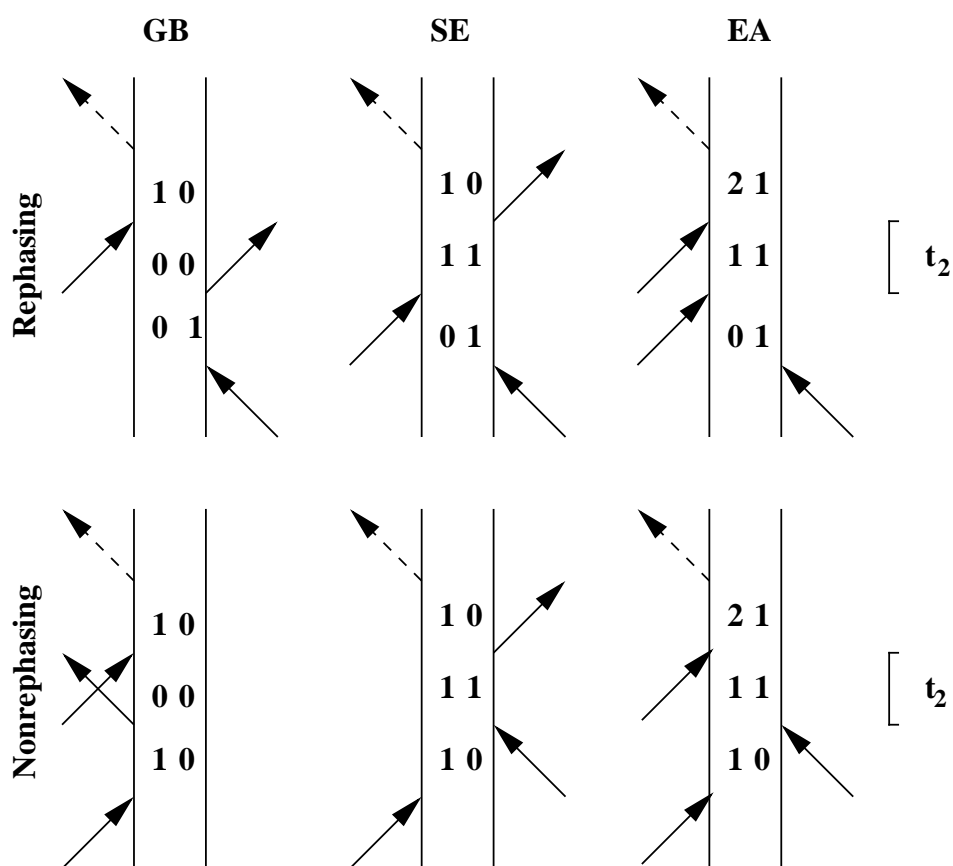


Multi-dimensional spectroscopy



Thomas la Cour Jansen
University of Groningen, 2009

Front cover: The double sided Feynman diagrams governing the two-dimensional infrared and optical experiments. Taken from Ref. [1].

These notes were prepared for the Graduate Course on Theoretical Chemistry and Spectroscopy in Han-sur-Lesse, 2009

Thomas la Cour Jansen,

Multi-dimensional spectroscopy,

University Groningen.

© T.l.C. Jansen, 2009

Contents

Contents	i
1 General Introduction	1
1.1 Multi dimensional spectroscopy	1
1.2 Suggested litterature	2
1.3 Outline	2
1.4 Acknowledgement	2
2 Time-dependent perturbation theory	5
2.1 Solving the Schrödinger equation	5
2.2 Calculating observables	7
2.3 Feynman diagrams and response functions	8
2.4 Feynman diagram selection	11
3 Multi-dimensional spectroscopies	15
3.1 Linear absorption (IR/vis)	15
3.2 Raman spectroscopy	15
3.3 Sum-frequency generation	16
3.4 Two-dimensional IR/vis spectroscopy	16
3.5 Two-dimensional Raman spectroscopy	19
3.6 Two-dimensional sum-frequency generation	19
3.7 Three-dimensional IR/vis spectroscopy	21
3.8 Exercises	21
4 Practical simulation of multi-dimensional spectra	23
4.1 Frequency fluctuations	23
4.2 The numerical integration of the Schrödinger equation scheme	24
4.2.1 Population transfer	25
4.2.2 Linear absorption	26
4.2.3 2DIR	26

CONTENTS

4.3 Dephasing and lineshapes	27
4.4 Reorientation	30
4.5 Population transfer	31
Bibliography	33

Chapter 1

General Introduction

In recent years multi-dimensional optical spectroscopies have been applied to unravel the structure and dynamics of complex systems. The observed spectra in these spectroscopies are often congested and difficult to interpret. Therefore, theoretical developments have been crucial. In these lecture notes the basic theory needed to describe and understand multi-dimensional spectra is given.

1.1 Multi dimensional spectroscopy

Experimentally the interactions and dynamics in complex systems manifest themselves in various types of traditional one-dimensional spectroscopies (as Nuclear Magnetic Resonance (NMR), Infrared spectroscopy (IR), Raman spectroscopy etc.). Phenomena such as line broadening and spectral shifts of the spectra contain information on both the dynamics and intermolecular interactions. However, the information obtained in this way is not very clear, since different physical phenomena give rise to very similar effects in the observed response. More information can be obtained using multi-dimensional spectroscopies.

In 1950 the NMR spin echo experiment for the first time allowed the determination of different line broadening mechanisms. [2] With two sets of radio frequency pulses it was possible first to induce Larmor precession of the nuclear spins with their individual Larmor frequencies and later revert the precession to produce a spin echo. In this way it was possible to distinguish between line broadening caused by slightly different Larmor frequencies due to different static environments around the nuclei and line broadening caused by interactions and motion on a timescale faster than the precession. This was the first example of a two-dimensional spectroscopy and developments in two-dimensional NMR now allow techniques with names such as COSY and NOESY to study complicated structures as those of proteins and even following protein folding processes on μs time scales. [3–5]

Theoretically, Feynman and coworkers showed that the concepts of NMR can be transferred

to optical spectroscopies. [6] This leads to the photon echo experiment, [7] which in particular with the use of two color pulses allows a full analysis of the optical dynamics analogous to that of two-dimensional NMR techniques. [8, 9] In 1993 Tanimura and Mukamel suggested the use of 2D Raman response to resolve the low frequency modes found in liquids [10] and a lot of effort was put into measuring this response. Both one- and two-dimensional response will be treated from a theoretical point of view in these notes. In recent years both two-dimensional versions of IR [11–13] , Raman [14, 15] and visual spectroscopy [16] were developed. The advantage of these methods is that they are able to probe motion on a much shorter timescales than NMR. The different nature of the methods means that they probe different kinds of motion and structural dynamics and hence the various multi-dimensional spectroscopies should rather be seen as complementing each other than competing. Pump-probe spectra [17] contain a subset of the information provided in the two-dimensional spectra and can be described by the same theoretical tools.

1.2 Suggested literature

So far no real books exist on multi-dimensional spectroscopy. However, a few useful texts covering the underlying non-linear optics does exist. The "Bible" is *Principles of Nonlinear Optical Spectroscopy* by Shaul Mukamel [18]. A supposedly more easily accessible text is the lecture notes *Principles of Nonlinear Optical Spectroscopy: A Practical Approach* also known as *Mukamel of Dummies* by Peter Hamm. *Nonlinear Optics* by Robert W. Boyd [19] is a useful book as well. There exist a number of review papers on multi-dimensional spectroscopy [20–24] and a complete issue of *Accounts of Chemical Research* is dedicated to this type of spectroscopy (Issue 9, 2009).

1.3 Outline

The remainder of these lecture notes is organized as follows. In Chapter 2 time-dependent perturbation theory is used to derive the response functions governing multi-dimensional spectroscopies and the double sided Feynman diagrams connected with these response functions will be discussed. In Chapter 3 the theory of the most common multi-dimensional spectroscopies will be discussed. A general method for simulating spectra will be described in Chapter 4.

1.4 Acknowledgement

I would like to thank Gerrit Groenenboom organizing the Han-sur-Lesse school for inviting me to give these lectures. I would also like to thank my ph.-d. supervisor Jaap G. Snijders,

who was teaching non-linear response functions when I attended the school in Han in 1998. He brought me into the field of multi-dimensional spectroscopy. Finally I would like to thank Santanu Roy for helping proof reading the notes.

Chapter 2

Time-dependent perturbation theory

In this Chapter we will apply time-dependent perturbation theory to derive response functions that govern multi-dimensional spectroscopy.

2.1 Solving the Schrödinger equation

When considering a quantum system that is changing in time we need to solve the time-dependent Schrödinger equation:

$$\frac{d\phi(t)}{dt} = -\frac{i}{\hbar}H(t)\phi(t). \quad (2.1)$$

The state of our system is determined by the time-dependent wavefunction $\phi(t)$ and the evolution is determined by the time-dependent Hamiltonian $H(t)$. In a spectroscopy experiment the Hamiltonian can typically be divided into two parts. The first part describes the system when it is not interacting with the applied light and is therefore typically *time-independent*. The other part governs the perturbation arising from the interaction between the system and the applied light, which is time-dependent. We denote these two parts of the Hamiltonian H_0 and $H_P(t)$ respectively.

The time-evolution of the state of a system with a time-independent Hamiltonian is trivial and given by

$$\phi(t) = \exp\left(-\frac{i}{\hbar}H_0(t-t_0)\right)\phi(t_0), \quad (2.2)$$

where t_0 is the initial time and t is the final time. The exponential operator is denoted the time-evolution operator

$$U(t, t_0) \equiv \exp\left(-\frac{i}{\hbar}H_0(t-t_0)\right). \quad (2.3)$$

For simplicity one can define a transformation from the original wavefunctions and operators (the Schrödinger picture) to a set where the trivial time-independent Hamiltonian is hidden in the operators (the interaction picture). The interaction picture makes the derivations shorter. The wavefunctions in the interaction picture are:

$$\phi_I(t) = \exp\left(\frac{i}{\hbar}H_0(t-t_0)\right)\phi(t) = U^\dagger(t, t_0)\phi(t) = \phi(t_0). \quad (2.4)$$

The operators in the interaction picture are given by:

$$\Omega^I(t) = \exp\left(\frac{i}{\hbar}H_0(t-t_0)\right)\Omega(t)\exp\left(-\frac{i}{\hbar}H_0(t-t_0)\right). \quad (2.5)$$

In the absence of time-dependent perturbation the wavefunction is therefore time-independent. In this case the interaction picture coincides with the so-called Heisenberg picture, where the wavefunction is constant and the time-dependence is in the operators.

The Schrödinger equation in the interaction picture reads:

$$\frac{d\phi_I(t)}{dt} = -\frac{i}{\hbar}H_P^I(t)\phi_I(t). \quad (2.6)$$

The only change in the wavefunction arise from the time dependent perturbation.

We will consider perturbations arising from interactions with an external electric field, $\vec{E}(t)$. In general the interaction between a system and an external electric field is given by an expansion in this field:

$$H_P^I(t) = \vec{\mu}^I \cdot \vec{E}(t) + \vec{\alpha}^I : \vec{E}(t)\vec{E}(t) + \dots \quad (2.7)$$

Here $\vec{\mu}$ is the transition dipole vector and $\vec{\alpha}$ is the transition polarizability tensor. Higher-order transition polarizabilities exist. These are in general not useful, but give rise to spectroscopic artifacts. The transition dipoles are typically connected with normal absorption spectroscopy and the transition polarizabilities with Raman spectroscopy. In the remainder of this Chapter we will assume that we are dealing with a type of spectroscopy, where we only need to account for the transition dipoles.

The time-dependent Schrödinger equation (Eq. (2.6)) can be rewritten as

$$\phi_I(t) = \phi_I(t_0) - \frac{i}{\hbar} \int_{t_0}^t d\tau_1 H_P^I(\tau_1)\phi_I(\tau_1). \quad (2.8)$$

It can now be solved in an iterative manner by plugging it into itself. To second order we get:

$$\phi_I(t) = \phi_I(t_0) - \frac{i}{\hbar} \int_{t_0}^t d\tau_1 H_P^I(\tau_1)\phi_I(t_0) + \left(-\frac{i}{\hbar}\right)^2 \int_{t_0}^t d\tau_2 \int_{t_0}^{\tau_2} d\tau_1 H_P^I(\tau_2)H_P^I(\tau_1)\phi_I(t_0). \quad (2.9)$$

To the m^{th} -order the solution is:

$$\begin{aligned} \phi_I(t) &= \phi_I(t_0) + \sum_{n=1}^{m-1} \left(-\frac{i}{\hbar}\right)^n \int_{t_0}^t d\tau_n \int_{t_0}^{\tau_n} d\tau_{n-1} \dots \int_{t_0}^{\tau_2} d\tau_1 H_P^I(\tau_n)H_P^I(\tau_{n-1}) \dots H_P^I(\tau_1)\phi_I(t_0) \\ &+ \left(-\frac{i}{\hbar}\right)^m \int_{t_0}^t d\tau_m \int_{t_0}^{\tau_m} d\tau_{m-1} \dots \int_{t_0}^{\tau_2} d\tau_1 H_P^I(\tau_m)H_P^I(\tau_{m-1}) \dots H_P^I(\tau_1)\phi_I(t_0) \end{aligned} \quad (2.10)$$

In the case of transition dipole interactions the n^{th} -order term corresponds to the wavefunction of a system that has interacted n times with the external electric field. For simplicity this n^{th} -order can be written:

$$\phi_I^{(n)}(t) = \left(-\frac{i}{\hbar}\right)^n \int_{t_0}^t d\tau_n \int_{t_0}^{\tau_n} d\tau_{n-1} \cdots \int_{t_0}^{\tau_2} d\tau_1 H_P^I(\tau_n) H_P^I(\tau_{n-1}) \cdots H_P^I(\tau_1) \phi_I(t_0). \quad (2.11)$$

This result can be transformed back to the usual Schrödinger picture by applying the reverse transformation

$$\phi^{(n)}(t) = \exp\left(-\frac{i}{\hbar}H_0(t-t_0)\right) \phi_I^{(n)}(t) = U(t, t_0) \phi_I^{(n)}(t). \quad (2.12)$$

2.2 Calculating observables

The time-dependence of an experimental observation is given by the expectation value of the corresponding operator Ω :

$$\langle \Omega \rangle(t) = \langle \phi_I | \Omega_I(t) | \phi_I \rangle = \langle \phi(t) | \Omega | \phi(t) \rangle \quad (2.13)$$

We will be interested in optical observables in particular the polarization, because an oscillating polarization will generate an electric field that we can measure as emitted light from the sample. The macroscopic polarization induced by external perturbations can be written in an expansion of the power dependence

$$P = \epsilon_0(\chi^{(1)}E + \chi^{(2)}E^2 + \chi^{(3)}E^3 + \cdots). \quad (2.14)$$

Here $\chi^{(1)}$ is the linear susceptibility and $\chi^{(2)}$ and $\chi^{(3)}$ are higher-order nonlinear susceptibilities. The electric fields are in fact vectors as is the polarization and the susceptibilities are tensors. The cartesian components denoted a through d can be used for the proper bookkeeping assuming implicit (Einstein) summation over these

$$P_a = \epsilon_0(\chi_{ab}^{(1)}E_b + \chi_{abc}^{(2)}E_bE_c + \chi_{abcd}^{(3)}E_bE_cE_d + \cdots). \quad (2.15)$$

In centrosymmetric systems, such as isotropic media, the even-order susceptibilities vanish due to the symmetry. These transform with an odd-order of the cartesian coordinates, which in centrosymmetric systems never belong to the total symmetric irreducible representation [19]. Or in other words, the polarization in systems with such symmetry must change sign when the optical electric fields are reversed and therefore the polarization generated by an even power of the electric field must vanish.

The macroscopic polarization is given by the ensemble average of the expectation value of the transition dipole

$$P(t) = \langle \langle \phi(t) | \mu | \phi(t) \rangle \rangle_E, \quad (2.16)$$

where $\langle \dots \rangle_E$ denote the ensemble average. To distinguish the order dependence of the electric field it is useful to define the n^{th} -order polarization which arise from n interactions with the external electric field.

$$P^{(n)}(t) = \sum_{m=0}^{m=n} \langle \langle \phi^{(n-m)}(t) | \mu | \phi^{(m)}(t) \rangle \rangle_E \quad (2.17)$$

Introducing separate numbering of the times in the bra (τ^B) and the ket (τ^K) side the wavefunctions can be explicitly written

$$\begin{aligned} P^{(n)}(t) &= \sum_{m=0}^{m=n} \left(\frac{i}{\hbar} \right)^{n-m} \left(-\frac{i}{\hbar} \right)^m \int_{t_0}^t d\tau_{n-m}^B \int_{t_0}^{\tau_{n-m}^B} d\tau_{n-m-1}^B \cdots \int_{t_0}^{\tau_2^B} d\tau_1^B \\ &\quad \int_{t_0}^t d\tau_m^K \int_{t_0}^{\tau_m^K} d\tau_{m-1}^K \cdots \int_{t_0}^{\tau_2^K} d\tau_1^K \\ &\quad \langle \langle \phi_I(t_0) | H_P^I(\tau_1^B) \cdots H_P^I(\tau_{n-m-1}^B) H_P^I(\tau_{n-m}^B) \mu(t) H_P^I(\tau_m^K) H_P^I(\tau_{m-1}^K) \cdots H_P^I(\tau_1^K) | \phi_I(t_0) \rangle \rangle_E. \end{aligned} \quad (2.18)$$

Assuming that $H_P^I(t) = \mu^I \cdot E(t)$ we get

$$\begin{aligned} P^{(n)}(t) &= \sum_{m=0}^{m=n} \left(\frac{i}{\hbar} \right)^{n-m} \left(-\frac{i}{\hbar} \right)^m \int_{t_0}^t d\tau_{n-m}^B \int_{t_0}^{\tau_{n-m}^B} d\tau_{n-m-1}^B \cdots \int_{t_0}^{\tau_2^B} d\tau_1^B \\ &\quad \int_{t_0}^t d\tau_m^K \int_{t_0}^{\tau_m^K} d\tau_{m-1}^K \cdots \int_{t_0}^{\tau_2^K} d\tau_1^K \\ &\quad \langle \langle \phi_I(t_0) | \mu^I(\tau_1^B) \cdots \mu^I(\tau_{n-m-1}^B) \mu^I(\tau_{n-m}^B) \mu^I(t) \mu^I(\tau_m^K) \mu^I(\tau_{m-1}^K) \cdots \mu^I(\tau_1^K) | \phi_I(t_0) \rangle \rangle_E \\ &\quad E(\tau_1^B) \cdots E(\tau_{n-m-1}^B) E(\tau_{n-m}^B) E(\tau_m^K) E(\tau_{m-1}^K) \cdots E(\tau_1^K) \end{aligned} \quad (2.19)$$

Or equivalently in the Schrödinger picture using that $U(t_1, t_2) = U^\dagger(t_2, t_1)$ and $U(t, t_0)U(t_0, t_2) = U(t_1, t_2)$

$$\begin{aligned} P^{(n)}(t) &= \sum_{m=0}^{m=n} \left(\frac{i}{\hbar} \right)^{n-m} \left(-\frac{i}{\hbar} \right)^m \int_{t_0}^t d\tau_{n-m}^B \int_{t_0}^{\tau_{n-m}^B} d\tau_{n-m-1}^B \cdots \int_{t_0}^{\tau_2^B} d\tau_1^B \\ &\quad \int_{t_0}^t d\tau_m^K \int_{t_0}^{\tau_m^K} d\tau_{m-1}^K \cdots \int_{t_0}^{\tau_2^K} d\tau_1^K \\ &\quad \langle \langle \phi(t_0) | U(t_0, \tau_1^B) \mu(\tau_1^B) \cdots \mu(\tau_{n-m-1}^B) U(\tau_{n-m-1}^B, \tau_{n-m}^B) \mu(\tau_{n-m}^B) U(\tau_{n-m}^B, t) \mu(t) \\ &\quad U(t, \tau_m^K) \mu(\tau_m^K) U(\tau_m^K, \tau_{m-1}^K) \mu(\tau_{m-1}^K) \cdots \mu(\tau_1^K) U(\tau_1^K, t_0) | \phi(t_0) \rangle \rangle_E \\ &\quad E(\tau_1^B) \cdots E(\tau_{n-m-1}^B) E(\tau_{n-m}^B) E(\tau_m^K) E(\tau_{m-1}^K) \cdots E(\tau_1^K) \end{aligned} \quad (2.20)$$

2.3 Feynman diagrams and response functions

Since the polarization might depend on electric fields applied at different times it is useful to define response functions that contain the information about what the polarization is

given that the interaction with the electric fields took place at specific times. The n^{th} -order polarization generated by interactions with external electric fields separated by the time delays t_1 to t_n is then

$$P^{(n)}(t, t_n, \dots, t_1) = S^{(n)}(t_n, t_{n-1}, \dots, t_1) E(t-t_n) E(t-t_n-t_{n-1}) \cdots E(t-t_n-t_{n-1}-\cdots-t_1). \quad (2.21)$$

Here the $S(t_n, t_{n-1}, \dots, t_1)$ is the response function. In simulations and thought experiments we can easily control when interactions with the external electric field can take place. We just assume that we apply a field that only has a value at very specific times. In practical experiments one can produce very short laser pulses, but their duration is limited by their frequency distribution. A δ -function shaped light pulse would contain all frequencies and is impossible to generate. The shorter the pulse is the bigger the bandwidth will be. If we want to interact with specific states selectively the limit on the pulse duration is one optical cycle. I.e. the pulse duration $\Delta t > 1/\omega$, where ω is the frequency of the exciting laser. In practice we therefore have to average over all possible interaction times.

$$P^{(n)}(t) = \int_0^\infty dt_n \int_0^\infty dt_{n-1} \cdots \int_0^\infty dt_1 S^{(n)}(t_n, t_{n-1}, \dots, t_1) \times E(t-t_n) E(t-t_n-t_{n-1}) \cdots E(t-t_n-t_{n-1}-\cdots-t_1). \quad (2.22)$$

For calculations we will typically start by assuming δ -function shaped light pulses and later consider the actual shape of the light pulses. We now need to consider the time ordering to connect Eqs. 2.22 and 2.20.

For the n^{th} -order the terms of Eq. (2.20) with m interactions on the bra side are the complex conjugate of the terms with m interactions on the ket side and $n-m$ interactions on the bra side. When n is odd there are therefore $(n+1)/2$ terms and when n is even there are $(n+2)/2$ terms. For these expressions there is no consideration of the time-ordering of the interactions to the bra side with respect to the interactions on the ket. For practical purposes such time ordering is useful to consider. It turns out that when there are m interactions on the ket there are $\binom{n}{m}$ different time-orderings possible. This gives a total of 2^{n-1} time-ordered terms. Each of these terms with a particular number of interactions on the ket and a particular time-ordering is connected with one so called Liouville space pathway. For each of these one can draw a double sided Feynman diagram showing the interactions and the time ordering.

Feynman diagram rules:

1. Vertical lines represent the time-evolution of the ket (drawn on the left) and the bra (drawn on the right). Time is running from the bottom to the top.
2. Interactions with the external electric field are represented by arrows. The last interaction, which is connected with the induced polarization emitting the signal, is indicated with a different arrow and is drawn on the left side of the diagram.

3. Each diagram has a sign $(-1)^m$, where m is the number of interactions from the bra. This is because the bra wavefunction contributes with a factor $(\frac{i}{\hbar})^{n-m}$ and the ket wavefunction contributes with a factor $(-\frac{i}{\hbar})^m$.
4. An arrow pointing to the right represents an electric field with $e^{-i\omega t + i\vec{k}\vec{r}}$, while an arrow pointing to the left represents an electric field with $e^{i\omega t - i\vec{k}\vec{r}}$. The real external electric field $E(t) = 2E_0(t) \cos(\omega t - \vec{k}\vec{r})$ can be separated into positive and negative frequency fields $E(t) = E_0(t)(e^{-i\omega t + i\vec{k}\vec{r}} + e^{i\omega t - i\vec{k}\vec{r}})$, where $E_0(t)$ is the pulse envelope. The frequency and wavevector of the emitted light is given by the sum of the input frequencies and wavevectors.
5. An arrow pointing towards the system represents a change to a higher-excited state and an arrow pointing away represents a change to a lower-excited state. This rule comes from the rotating wave approximation requiring that the interactions should be resonant (see below). The last interaction is connected with emission of the signal and always point away from the system.
6. Before the first interaction the wavefunction connected with each line should be that of the initial (ground) state and after the last interaction the two wavefunctions should be identical.

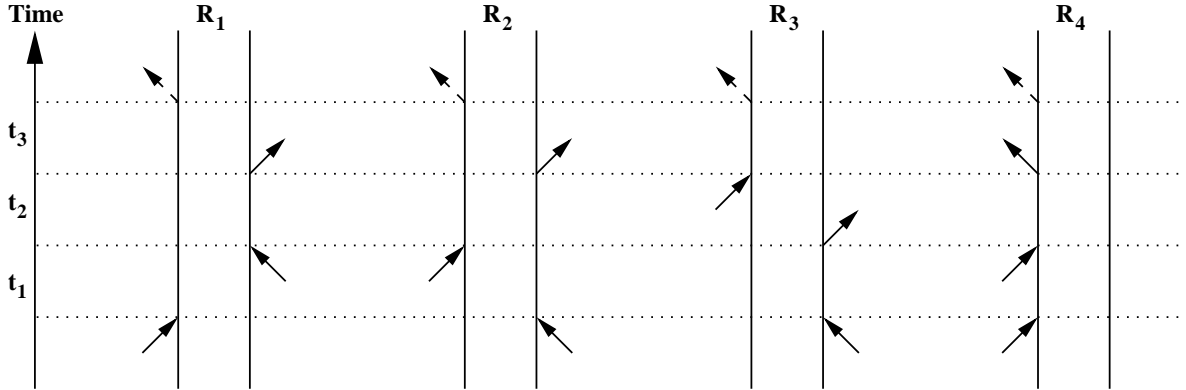


FIGURE 2.1: Four of the eight doublesided Feynman diagrams connected with the third-order response functions. The other four are the complex conjugate of these four.

Writing the response function corresponding to a particular diagram is now trivial. The sign is $(-1)^m$, when m is the number of interactions on the right. Writing from right to left one start at time 0 with $|\phi(0)\rangle$ and follow the left side forward in time. For each interaction one write a dipole operator μ and for each interval between the interactions one write a time-evolution operator $U(t + t_1, t)$. After the last interaction one goes back in time along the right side following the same rules and remembering that the time now progress backwards.

Finally, one ends with the ground state wavefunction again $\langle\phi(0)|$. In practice the sign is frequently reversed. This is a matter of convention and only depends on whether one wants to consider the absorption or transmission. Here the absorption convention will be used.

Experimentally it is possible not only to separate response at different orders of interaction, but by controlling the laser central frequencies, the direction of the laser beams and the order of the laser pulses one can select subsets of the Feynman diagrams.

2.4 Feynman diagram selection

In a multi-pulse experiment with n different incoming laser beams the electric field is

$$E(t) = \sum_{j=1}^n E_j(t) (e^{-i\omega_j t + i\bar{k}_j \bar{r}} + e^{i\omega_j t - i\bar{k}_j \bar{r}}). \quad (2.23)$$

The envelope functions E_j contain the information about the amplitude of pulse j at different times. In the impulsive limit this function is approximated by a delta function. This approximation, which is extremely useful for practical calculations, can only be done when one at the same time considers the consequences for phase matching and energy conservation.

When the wavevectors of the applied laser beams are slightly different, signals originating from different Feynman diagrams will be emitted in different directions.

$$\bar{k}_s = \sum_{j=1}^n \pm \bar{k}_j. \quad (2.24)$$

The sign depends on which part of the electric field is interacting. One can therefore select the signal that originates from interacting exactly once with each laser field by detecting the signal in the proper direction. Other signals with multiple interactions with one beam will be generated in experiments, but one can choose not to measure this signal. In this way one can control exactly which beam is interacting with the sample at what time.

The central frequency of the emitted field will likewise be given by

$$\omega_s = \sum_{j=1}^n \pm \omega_j. \quad (2.25)$$

The sign for each frequency is the same as for the wavevector. In order to use the impulsive limit we need to disregard the Feynman diagrams that are off-resonant. Let's consider the linear response of a two-level system as a simple example. The response function for such a system is

$$S^{(1)}(t_1) = -\frac{i}{\hbar} \mu^2 e^{-\frac{i}{\hbar} \epsilon t_1} e^{-\Gamma t_1} + c.c. \quad (2.26)$$

Here μ is the transition dipole, ϵ the energy difference between the two levels and Γ is the lifetime of the excited state. The resulting polarization is

$$P^{(1)}(t) = \int_0^\infty dt_1 E(t - t_1) S^{(1)}(t_1). \quad (2.27)$$

We assume that the field is

$$E(t) = E_0(t)(e^{-i\omega_1 t + i\bar{k}_1 \bar{r}} + e^{i\omega_1 t - i\bar{k}_1 \bar{r}}). \quad (2.28)$$

Filling in the electric field gives two terms

$$P^{(1)}(t) = -\frac{i}{\hbar} \mu^2 \int_0^\infty dt_1 e^{-\frac{i}{\hbar} \epsilon t_1} e^{-\Gamma t_1} e^{-i\omega_1(t-t_1) + i\bar{k}_1 \bar{r}} E_0(t - t_1) + c.c. \quad (2.29)$$

$$-\frac{i}{\hbar} \mu^2 \int_0^\infty dt_1 e^{-\frac{i}{\hbar} \epsilon t_1} e^{-\Gamma t_1} e^{i\omega_1(t-t_1) - i\bar{k}_1 \bar{r}} E_0(t - t_1) + c.c. \quad (2.30)$$

We collect the terms oscillating in the time t_1 and find

$$P^{(1)}(t) = -\frac{i}{\hbar} \mu^2 e^{-i\omega_1 t + i\bar{k}_1 \bar{r}} \int_0^\infty dt_1 e^{-i(\frac{\epsilon}{\hbar} - \omega_1)t_1} e^{-\Gamma t_1} E_0(t - t_1) + c.c. \quad (2.31)$$

$$-\frac{i}{\hbar} \mu^2 e^{i\omega_1 t - i\bar{k}_1 \bar{r}} \int_0^\infty dt_1 e^{-i(\frac{\epsilon}{\hbar} + \omega_1)t_1} e^{-\Gamma t_1} E_0(t - t_1) + c.c. \quad (2.32)$$

When the laser frequency is close to resonance with the two-level system, i.e. $\omega_1 \approx \frac{\epsilon}{\hbar}$ the integrand of the first term is slowly oscillating, while the integrand of the second term is rapidly oscillating. For finite pulse durations the second term will therefore be very small and should be disregarded, when one uses the impulsive limit which would wrongfully give a contribution from this term otherwise. Neglecting such off-resonant terms is denoted the rotating wave approximation (RWA). The two contributions from this example are also illustrated in Figure 2.2. The physical interpretation is that in the first diagram the left side is brought from the ground state to the excited state. In the second diagram the interaction should de-excite the system, but this is in the ground state and cannot be lowered. Therefore this diagram should be disregarded.

One should be aware that when the applied laser fields are overlapping in time (i.e. the actual duration of the pulses is longer than the delay between them) it is not possible to control the time-ordering of the interactions experimentally and artifacts can arise from diagrams that one would otherwise have disregarded. Such artifacts can only be accounted for by using the actual pulse envelopes instead of the impulsive limit. This is, however, in practice done very seldom because the pulse envelopes varies in different experimental setups.

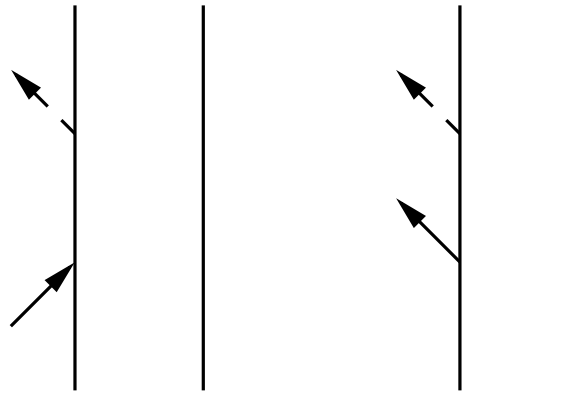


FIGURE 2.2: *The Feynman diagrams connected with the first-order response functions. In the left diagram the first interacting field has the phase $e^{-i\omega_1(t-t_1)+i\bar{k}_1\bar{r}}$, while the phase in the right diagram is $e^{i\omega_1(t-t_1)-i\bar{k}_1\bar{r}}$.*

Chapter 3

Multi-dimensional spectroscopies

In this Chapter we will discuss the theory behind the most common multi-dimensional spectroscopies. For completeness a few one-dimensional spectroscopies will be discussed first.

3.1 Linear absorption (IR/vis)

The Feynman diagram corresponding to linear absorption is given in Figure 3.1. The fields may be infrared or visual allowing the probe of vibrational excitations or electronic excitations respectively. In both cases the response function is

$$S^{(1)}(t) = -\frac{i}{\hbar} \langle \phi_0(0) | \mu(t) e^{-\frac{i}{\hbar} H t} \mu(0) | \phi_0(0) \rangle e^{-\Gamma t} \quad (3.1)$$

The last term is an *ad hoc* lifetime of the excited state. The actual spectrum is given by the imaginary part of the Fourier transform with respect to t . Assuming a number of eigen states with frequencies ω_i and transition-dipole μ_i the spectrum is then given by a sum of Lorentzians

$$I(\omega) = \sum_i \frac{\mu_i^2}{\pi} \frac{\Gamma}{(\omega - \omega_i)^2 + \Gamma^2}. \quad (3.2)$$

3.2 Raman spectroscopy

In Raman spectroscopy the excitation is happening through the interaction with two off-resonant fields (see Figure 3.1). The perturbation $H_P(t)$ is therefore determined by the transition-polarizability, i.e. $\bar{\alpha} : \vec{E}(t) \vec{E}(t)$. The response function is therefore simply

$$S^{(1)}(t) = -\frac{i}{\hbar} \langle \phi_0(0) | \alpha(t) e^{-\frac{i}{\hbar} H t} \alpha(0) | \phi_0(0) \rangle e^{-\Gamma t}. \quad (3.3)$$

The spectrum for a collection of eigen states with frequencies ω_i and transition-polarizabilities α_i is

$$I(\omega) = \sum_i \frac{\alpha_i^2}{\pi} \frac{\Gamma}{(\omega - \omega_i)^2 + \Gamma^2}. \quad (3.4)$$

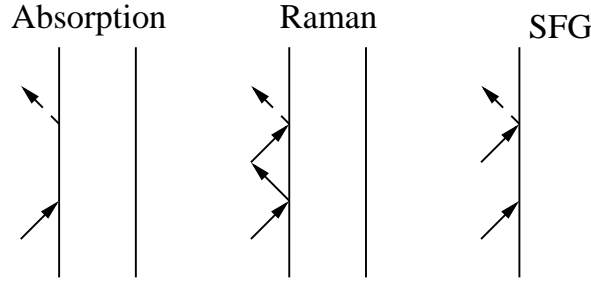


FIGURE 3.1: *The Feynman diagrams connected with linear absorption, Raman spectroscopy and sum-frequency generation (SFG).*

Since the transition-polarizabilities are tensors depending on the polarization of the laser light one can probe different parts of this by varying the polarization of the light. In isotropic media there are two linear independent signals that one can measure. A typical choice is using the anisotropic and the isotropic polarization setup.

3.3 Sum-frequency generation

Sum-frequency generation (SFG) is like a hybrid between linear absorption and Raman combining one resonant dipole interaction with an off-resonant Raman interaction (see Figure 3.1). The most obvious advantage of SFG is that it is a second-order spectroscopy involving three external laser fields. It therefore vanishes in systems with inversion symmetry. It is therefore especially useful in the study of surfaces. The response function is

$$S^{(1)}(t) = -\frac{i}{\hbar} \langle \phi_0(0) | \alpha(t) e^{-\frac{i}{\hbar} H t} \mu(0) | \phi_0(0) \rangle e^{-\Gamma t}. \quad (3.5)$$

The spectrum for a collection of eigen states with frequencies ω_i and transition-polarizabilities α_i is

$$I(\omega) = \sum_i \frac{\alpha_i \mu_i}{\pi} \frac{\Gamma}{(\omega - \omega_i)^2 + \Gamma^2}. \quad (3.6)$$

The polarization of the light can be used to determine the angle between the surface and the transition dipole.

3.4 Two-dimensional IR/vis spectroscopy

In two-dimensional infrared and visual spectroscopy three laser pulses are applied at different time delays. Usually the second time delay is fixed. Usually two phase-matching conditions are used and all laser frequencies are equal. The Feynman diagrams selected in this situation

are given in Figure 3.2. The rephasing (also called photon echo) diagrams arise in the phase-matching direction $\bar{k}_I = -\bar{k}_1 + \bar{k}_2 + \bar{k}_3$ and the nonrephasing diagrams arise in the phase-matching direction $\bar{k}_{II} = +\bar{k}_1 - \bar{k}_2 + \bar{k}_3$. This corresponds to changing the time-ordering of the first two-interactions. In typical experiments the signal from these two directions are added up. A third phase-matching setup is $\bar{k}_{III} = +\bar{k}_1 + \bar{k}_2 - \bar{k}_3$, but this is not very frequently used. One interesting application is, however, the detection of electron correlations [25].

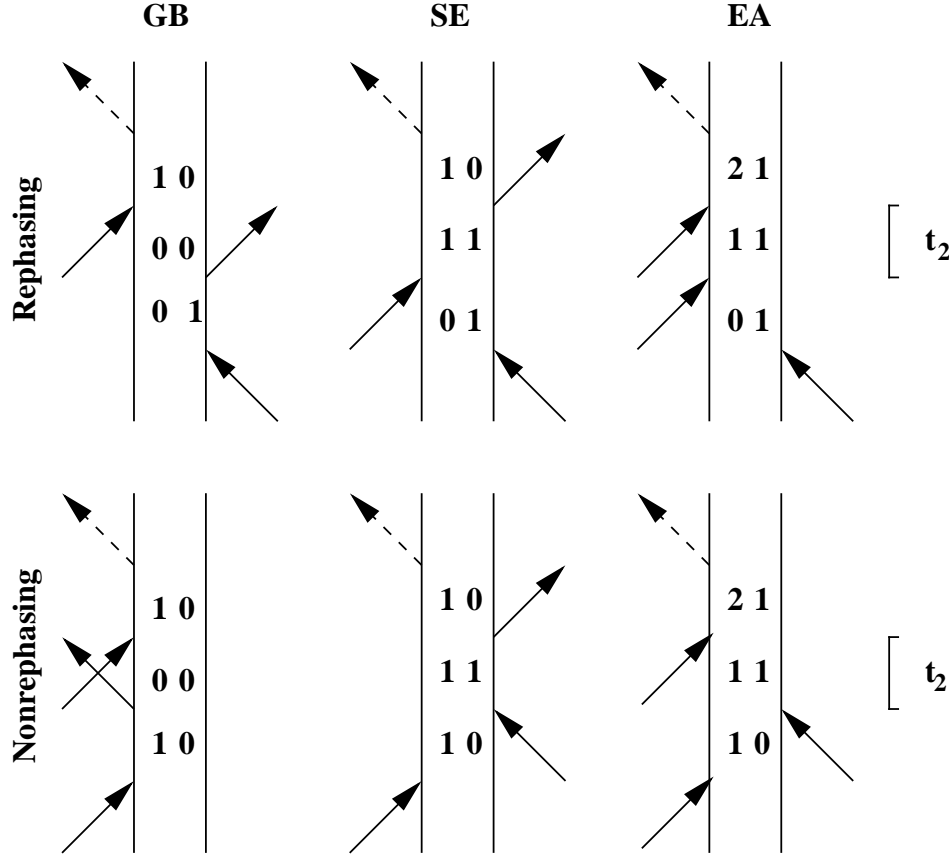


FIGURE 3.2: The Feynman diagrams connected with two-dimensional infrared and visible spectroscopy. The numbers indicate the excitation level of the wavefunctions during the different time-intervals.

For both phase matching conditions k_I and k_{II} there are three Feynman diagrams. In the first denoted the ground state bleach (GB) the system is in the ground state (symbolized by a 0 in Figure 3.2) during the second time delay. During the two other time-delays one side is in the ground state and the other in a single excited state. This is also called a coherence between these two states. The time dependence of such a coherence is $e^{-\frac{i}{\hbar}(\epsilon_B - \epsilon_K)t}$ where ϵ_B and ϵ_K are the energies connected with the bra and ket wave functions. In the stimulated emission (SE) and excited state absorption (EA) diagrams the system is in a singly excited

state during the second time delay both on the ket and the bra side. In the SE diagram the system is in a coherence between the ground state and a singly excited state during the last time delay, while for the EA diagram the system is in a coherence between a single excited and a doubly excited state. According to the Feynman rules the sign of the EA diagram is opposite to that of the GB and SE.

Just as for the linear response the signal is Fourier transformed to obtain a spectrum. By Fourier transforming with respect to the first and third time delay one obtains a two dimensional spectrum as illustrated in Figure 3.3 for two coupled three level systems. The frequency connected with the first time delay is ω_1 and the frequency connected with the third time delay is ω_3 . The diagonal peaks (A) arise from the GB and SE diagrams when the system is in the same coherence during the two time delays. The cross peaks (C) arise from the same diagrams, when the system is in the coherence between one single excited state and the ground state during the first time delay and in the coherence between the other single excited state and the ground state during the third time delay. The peaks arising from the EA diagram are typically found slightly below the GB and SE peaks. This is because in the EA diagram the system is in a coherence between a double excited and a single excited state during the last time delay. The energy of the double excited state at least in vibrational systems is typically slightly lower than twice the energy of the single excited state. This difference is denoted the anharmonicity. If the anharmonicity is zero the peaks from the EA diagram will fall on top of the GB and SE diagrams and cancel perfectly with them leaving no detectable signal.

The delay t_2 is denoted the waiting time. This time can be varied and by studying the changes of the spectrum as the waiting time is changed one can obtain dynamical information. While two-dimensional IR/visual spectroscopy reveal coupling information that is not present in the corresponding one-dimensional spectrum, the waiting time is the true advantage. The waiting time can be used to study all kinds of dynamical processes as rotational motion, chemical exchange, population transfer and spectral diffusion [1].

The cross peaks in the two-dimensional spectra reveal information on the coupling between different states. While the overtone peaks reveal information on the anharmonicity, these peaks are often rather an annoyance than something providing useful information. The relative orientation between transition dipoles can be obtained by choosing the polarization of the laser pulses [26]. Most frequently two polarization configurations are used. In the first naturally called the parallel polarization spectrum all laser field polarizations are parallel. In the second the first two laser field polarizations are parallel and the last field is polarized perpendicular to the two first and the observed signal has a polarization parallel with the last laser field. This configuration is denoted the perpendicular polarization spectrum.

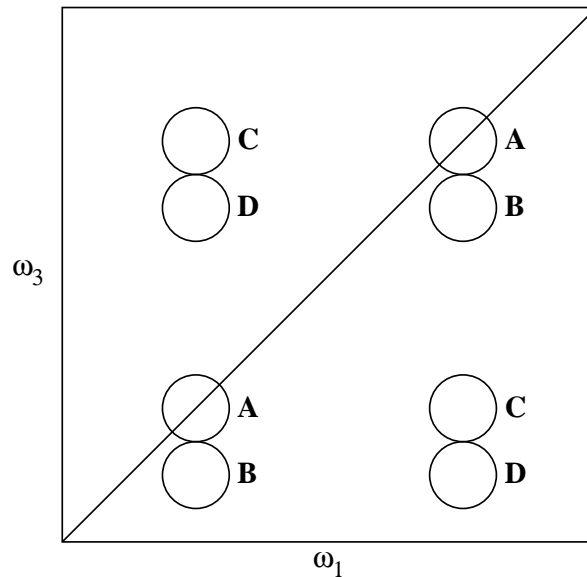


FIGURE 3.3: A schematic representation of a two-dimensional spectrum for a two coupled three level systems. A, B, C and D are diagonal peaks (from GB and SE), diagonal overtone peaks (from EA), cross peaks (from GB and SE) and cross peak overtones (from EA). Frequently the ω_1 and ω_3 axes are exchanged. The A and C peaks have the opposite sign of the B and D peaks.

3.5 Two-dimensional Raman spectroscopy

In two-dimensional Raman spectroscopy five laser pulses are involved in three Raman interactions. In Figure 3.4 the Feynman diagrams corresponding to the signals in the $\bar{k}_s = \bar{k}_1 - \bar{k}_2 + \bar{k}_3 - \bar{k}_4 + \bar{k}_5$ phase matching directions are given. While great effort was put in the detection and modeling of the two-dimensional Raman response it has only been detected for very few systems. The signal is very weak and so called cascaded responses originating from two connected third-order Raman processes at different positions in the sample are contaminating the signal [27–30]. Since these cascades involves two molecules at different locations in the sample it scales differently with sample size than the two-dimensional Raman signal that originates from one position. One can therefore in principle make the sample more dilute or the sample cell thinner. This will also make the signal smaller, but maybe with future technology these problems can be overcome.

3.6 Two-dimensional sum-frequency generation

The two-dimensional sum-frequency generation (2DSFG) is in many ways similar to the two-dimensional IR/vis spectroscopy. The Feynman diagrams are given in Figure 3.5. Just as

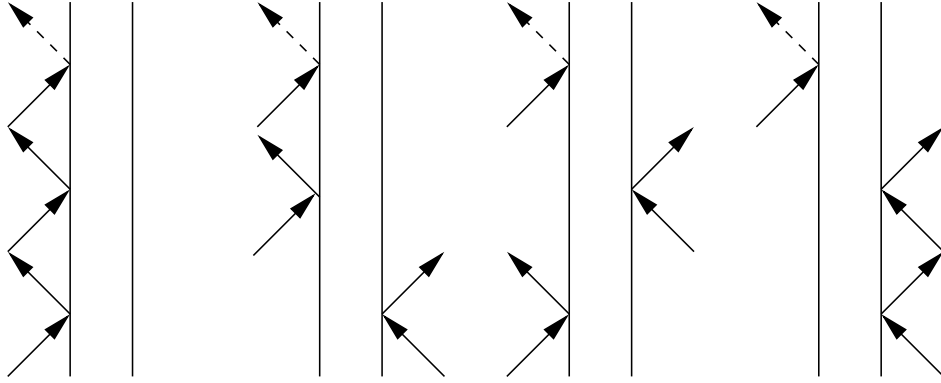


FIGURE 3.4: *The Feynman diagrams connected with two-dimensional Raman spectroscopy.*

for normal SFG the major difference is the symmetry determined selection rules. 2DSFG is therefore suitable for studying structure and dynamics of surfaces and interfaces [31]. So far only very few applications of 2DSFG have been made, but in the future one can expect to see many.

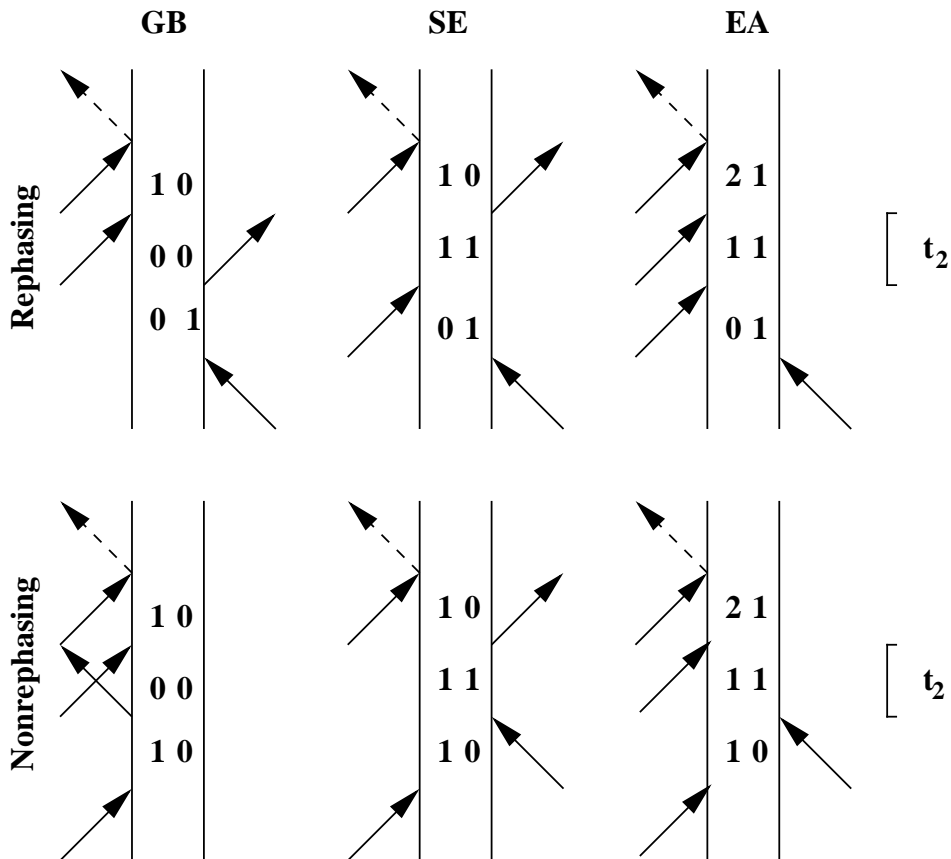


FIGURE 3.5: *The Feynman diagrams connected with two-dimensional sum-frequency generation spectroscopy.*

3.7 Three-dimensional IR/vis spectroscopy

So far only very few experiments have been done for three-dimensional IR/vis spectroscopy and it has only been realized for infrared laser fields [32]. This, more exotic spectroscopy, is limited by relatively small signals and is complicated by the fact that triple-excited states will contribute. For a simple anharmonic oscillator system using the phase matching $\bar{k}_s = \bar{k}_1 - \bar{k}_2 + \bar{k}_3 - \bar{k}_4 + \bar{k}_5$ the five Feynman diagrams in Figure 3.6 will contribute. These are all located at different positions in the three-dimensional spectrum if the anharmonicity is nonzero. As for two-dimensional spectroscopy the signal will vanish for a harmonic oscillator due to destructive interference of the peaks.

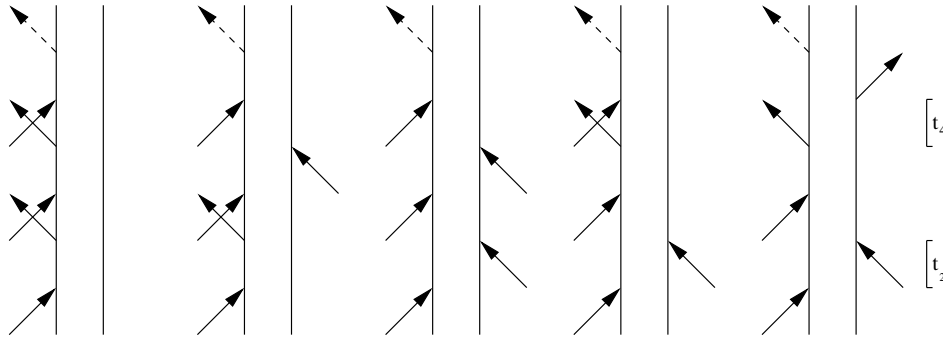


FIGURE 3.6: *The Feynman diagrams connected with three-dimensional infrared and visible spectroscopy.*

3.8 Exercises

1. Write down the expressions for the Feynman diagrams for the two-dimensional IR/vis spectra.
2. Find the excitation level for the wavefunctions at different times in the Feynman diagrams for the three-dimensional spectra in Figure 3.6.

Chapter 4

Practical simulation of multi-dimensional spectra

In the previous Chapter the Feynman diagrams governing the different multi-dimensional spectra were given and the explicit expressions for the linear response was given. It was assumed that the Hamiltonian could be seen as constant during the experiments and the transition dipoles were constant as well. In reality the systems considered are not isolated, but in contact with a bath that is not explicitly part of the Hamiltonian. The consequence is that the Hamiltonian of the becomes time-dependent. Furthermore the transition dipoles can change as well for example as the molecules rotate the transition dipoles will rotate along. This situation, which seemingly is much more complicated than the actual problem that was solved in Chapter 2, can be accounted for rather easily. In this Chapter the practical simulation of multi-dimensional spectra in dynamic systems will be treated. The approach discussed here is not the only available approach, however, in contrast to for example the well known second-order cumulant approach [33] it does allow the treatment of very general situations such as chemical exchange. More exact methods as the hierarchical equations of motion (HEOM) [34, 35] are much more demanding computationally and have only been applied to very small systems.

4.1 Frequency fluctuations

If the Hamiltonian is fluctuating the time-evolution operator used in the response functions discussed in the previous chapters simply have to be exchanged with the formal solution of the time-dependent Schrödinger equation

$$U(t + \Delta t, t) = \exp_+ \left(-\frac{i}{\hbar} \int_0^{\Delta t} d\tau H(t + \tau) \right). \quad (4.1)$$

For the transition-dipoles the magnitude and orientation at the instant of the interaction should be used. The fluctuations can be found by doing molecular dynamics simulations and connecting the frequencies with the changes in the environment through *ab initio* calculations or through Stark effect mappings that connect the local electric field on a vibration or molecule with the frequency of the studied vibration or electronic excitation [36–40]. Alternatively stochastic models can be constructed for model calculations.

4.2 The numerical integration of the Schrödinger equation scheme

In the following a collection of three level systems will be considered. The approach can in principle be generalized to systems with more levels, however, for treating two-dimensional optical spectroscopy one cannot reach these levels. For three-dimensional spectroscopy four levels are accessible. For electronic systems two levels will be sufficient. The scheme is denoted the numerical integration of the Schrödinger equation (NISE) scheme [41]. We employ the simplest possible exciton Hamiltonian for a collection of N floating oscillators of the form

$$\mathbf{H}(t) = \sum_{i=1}^N \left[\epsilon_i(t) \mathbf{b}_i^\dagger \mathbf{b}_i - \frac{\Delta_i(t)}{2} \mathbf{b}_i^\dagger \mathbf{b}_i^\dagger \mathbf{b}_i \mathbf{b}_i \right] + \sum_{i,j} J_{ij}(t) \mathbf{b}_i^\dagger \mathbf{b}_j + \sum_{i=1}^N \vec{\mu}_i(t) \cdot \vec{E}(t) \left[\mathbf{b}_i^\dagger + \mathbf{b}_i \right]. \quad (4.2)$$

Here $\epsilon_i(t)$ and $\Delta_i(t)$ are the fluctuating frequency and anharmonicity respectively, of mode i , $J_{ij}(t)$ is the fluctuating coupling between two modes, and \mathbf{b}_i^\dagger and \mathbf{b}_i are the usual Bose creation and annihilation operators. The modes interact with the applied electric field $\vec{E}(t)$ through the transition dipoles $\vec{\mu}_i(t)$, which might fluctuate in time as well. In the Hamiltonian (Eq. (4.2)) states with a different number of excitations are only coupled when an external field is present. When the external field is vanishing, it is therefore block diagonal and the different blocks can be treated separately. We denote the block concerning the ground state \mathbf{H}^{gg} , the singly excited states \mathbf{H}^{ee} , and the doubly excited states \mathbf{H}^{ff} . We will consider interactions with an external electric field tuned to be resonant with the change of one excitation quantum. In this case we need the transition dipoles between the ground state and the singly excited states $\boldsymbol{\mu}^{ge}$ and those between the singly and doubly excited states $\boldsymbol{\mu}^{ef}$.

The time-dependent Schrödinger equation

$$\frac{\partial}{\partial t} \Phi(t) = -\frac{i}{\hbar} \mathbf{H}(t) \Phi(t) \quad (4.3)$$

is solved for each block independently. Here $\Phi(t)$ is the wave function at time t . The evolution of all possible states can be tracked if the evolution is known in an arbitrary, but fixed and complete basis. We will utilise the site basis, where the excitations are localised on the amide I sites. If a system was in the site basis state $\phi_i = \mathbf{b}_i^\dagger |g\rangle$ at time zero it will have evolved

into $\Phi_i(t)$ at time t . This wavefunction can be written in terms of the original fixed site basis functions ϕ for the considered excitation manifold.

$$\Phi_i(t) = \sum_j \phi_j c_{ji}(t) \quad (4.4)$$

For $t=0$ the expansion coefficients fulfill $c_{ji}(0) = \delta_{ji}$. Upon insertion of Eq. (4.4) in the time-dependent Schrödinger equation, an equation for the expansion coefficients is obtained:

$$\frac{\partial}{\partial t} c_{ik}(t) = -\frac{i}{\hbar} \sum_j H_{ij}(t) c_{jk}(t) \quad (4.5)$$

which can be written in matrix form

$$\frac{\partial}{\partial t} \mathbf{c}(t) = -\frac{i}{\hbar} \mathbf{H}(t) \mathbf{c}(t). \quad (4.6)$$

For numerical integration of this equation using small time increments, the Hamiltonian can be treated as constant during each integration step. The integration over one such timestep of duration Δt yields

$$\mathbf{c}((n+1)\Delta t) = \exp\left(-\frac{i}{\hbar} \mathbf{H}(n\Delta t) \Delta t\right) \mathbf{c}(n\Delta t) \equiv \mathbf{U}((n+1)\Delta t, n\Delta t) \mathbf{c}(n\Delta t), \quad (4.7)$$

with the integer n labeling the timestep. By combining all time evolution operators $\mathbf{U}((j+1)\Delta t, j\Delta t)$ from the selected starting time to all other times we have

$$\mathbf{U}(n\Delta t, 0) = \left[\prod_{m=1}^{m=n} \mathbf{U}(m\Delta t, (m-1)\Delta t) \right]. \quad (4.8)$$

The product \prod denotes the time-ordered operation from the left with increasing m . The time-evolution matrices between two arbitrary points in time is found using their unitary property $\mathbf{U}(t_1, t_0) = \mathbf{U}(t_1, 0) \mathbf{U}^\dagger(t_0, 0)$. Adding gg , ee or ff to the matrices indicates which block of the Hamiltonian is used. The approach described here and the Hamiltonian employed allow for the description of population transfer within the exciton manifolds.

4.2.1 Population transfer

The population transfer between two states in the site basis is calculated using

$$P_{ba}(t) = \langle |\langle \phi_b | U(t, 0) | \phi_a \rangle|^2 \rangle_E, \quad (4.9)$$

where a is the initial state and b is the final state. The ensemble average, $\langle \dots \rangle_E$ is obtained by summing over the contributions from different realizations of the fluctuations. One way to do this is by using different configurations along a MD trajectory. At zero time delay the population will be in the initial state, i.e., $P_{ab}(0) = \delta_{ab}$ and at infinite delay the population will be equally distributed over all states, i.e. $P_{ab}(0) = 1/N$. The latter is due to the classical treatment of the bath, which is valid in the high temperature limit, when the energy difference between the states is smaller than the thermal energy.

4.2.2 Linear absorption

The linear absorption is given by the Fourier transform of the two-point correlation function of the transition dipole

$$I(\omega) = \text{Im} \int_0^\infty dt_1 \frac{i}{\hbar} \langle \langle g | \boldsymbol{\mu}^{ge}(\tau_2) \mathbf{U}^{ee}(\tau_2, \tau_1) \boldsymbol{\mu}^{eg}(\tau_1) | g \rangle \rangle_E \exp(-i\omega t_1) \Gamma_{LA}(t_1). \quad (4.10)$$

Here τ_2 and τ_1 are the times, when the system interacts with the external field and t_1 is the time between these interactions ($t_1 = \tau_2 - \tau_1$). The vibrational lifetime is accounted for by the relaxation factor

$$\Gamma_{LA}(t_1) = \exp(-t_1/2T_1), \quad (4.11)$$

where T_1 is the lifetime of the singly excited states.

4.2.3 2DIR

The 2DIR spectrum is given as the sum of the signal emitted in the directions with wave vectors $\bar{k}_I = -\bar{k}_1 + \bar{k}_2 + \bar{k}_3$ and $\bar{k}_{II} = \bar{k}_1 - \bar{k}_2 + \bar{k}_3$, where \bar{k}_1 , \bar{k}_2 , and \bar{k}_3 are the wave vectors of the incoming fields. \bar{k}_I is the photon-echo signal and \bar{k}_{II} is the non-rephasing signal. Each of these signals contains three contributions from distinct Liouville space pathways: ground state bleach (GB), stimulated emission (SE) and excited state absorption (EA) [18,42]. These are given by

$$\begin{aligned} S_{GB}^{(I)}(t_3, t_2, t_1) &= - \left(\frac{i}{\hbar} \right)^3 \langle \langle g | \boldsymbol{\mu}^{ge}(\tau_1) \mathbf{U}^{ee}(\tau_1, \tau_2) \boldsymbol{\mu}^{eg}(\tau_2) \boldsymbol{\mu}^{ge}(\tau_4) \mathbf{U}^{ee}(\tau_4, \tau_3) \boldsymbol{\mu}^{eg}(\tau_3) | g \rangle \rangle_E \\ &\quad \times \Gamma(t_3, t_2, t_1) \\ S_{SE}^{(I)}(t_3, t_2, t_1) &= - \left(\frac{i}{\hbar} \right)^3 \langle \langle g | \boldsymbol{\mu}^{ge}(\tau_1) \mathbf{U}^{ee}(\tau_1, \tau_3) \boldsymbol{\mu}^{eg}(\tau_3) \boldsymbol{\mu}^{ge}(\tau_4) \mathbf{U}^{ee}(\tau_4, \tau_2) \boldsymbol{\mu}^{eg}(\tau_2) | g \rangle \rangle_E \\ &\quad \times \Gamma(t_3, t_2, t_1) \\ S_{EA}^{(I)}(t_3, t_2, t_1) &= \left(\frac{i}{\hbar} \right)^3 \langle \langle g | \boldsymbol{\mu}^{ge}(\tau_1) \mathbf{U}^{ee}(\tau_1, \tau_4) \boldsymbol{\mu}^{ef}(\tau_4) \mathbf{U}^{ff}(\tau_4, \tau_3) \boldsymbol{\mu}^{fe}(\tau_3) \mathbf{U}^{ee}(\tau_3, \tau_2) \boldsymbol{\mu}^{eg}(\tau_2) | g \rangle \rangle_E \\ &\quad \times \Gamma(t_3, t_2, t_1) \\ S_{GB}^{(II)}(t_3, t_2, t_1) &= - \left(\frac{i}{\hbar} \right)^3 \langle \langle g | \boldsymbol{\mu}^{ge}(\tau_4) \mathbf{U}^{ee}(\tau_4, \tau_3) \boldsymbol{\mu}^{eg}(\tau_3) \boldsymbol{\mu}^{ge}(\tau_2) \mathbf{U}^{ee}(\tau_2, \tau_1) \boldsymbol{\mu}^{eg}(\tau_1) | g \rangle \rangle_E \\ &\quad \times \Gamma(t_3, t_2, t_1) \\ S_{SE}^{(II)}(t_3, t_2, t_1) &= - \left(\frac{i}{\hbar} \right)^3 \langle \langle g | \boldsymbol{\mu}^{ge}(\tau_2) \mathbf{U}^{ee}(\tau_2, \tau_3) \boldsymbol{\mu}^{eg}(\tau_3) \boldsymbol{\mu}^{ge}(\tau_4) \mathbf{U}^{ee}(\tau_4, \tau_1) \boldsymbol{\mu}^{eg}(\tau_1) | g \rangle \rangle_E \\ &\quad \times \Gamma(t_3, t_2, t_1) \\ S_{EA}^{(II)}(t_3, t_2, t_1) &= \left(\frac{i}{\hbar} \right)^3 \langle \langle g | \boldsymbol{\mu}^{ge}(\tau_2) \mathbf{U}^{ee}(\tau_2, \tau_4) \boldsymbol{\mu}^{ef}(\tau_4) \mathbf{U}^{ff}(\tau_4, \tau_3) \boldsymbol{\mu}^{fe}(\tau_3) \mathbf{U}^{ee}(\tau_3, \tau_1) \boldsymbol{\mu}^{eg}(\tau_1) | g \rangle \rangle_E \\ &\quad \times \Gamma(t_3, t_2, t_1) \end{aligned} \quad (4.12)$$

The vibrational lifetime is included in an *ad hoc* way through the relaxation factor

$$\Gamma(t_3, t_2, t_1) = \exp(-(t_3 + 2t_2 + t_1)/2T_1). \quad (4.13)$$

τ_1 through τ_4 are the times for interactions with the external electric field and t_1 through t_3 are the time delays between these (i.e. $t_1 = \tau_2 - \tau_1$, $t_2 = \tau_3 - \tau_2$, and $t_3 = \tau_4 - \tau_3$). T_1 and T_2 are the lifetimes of the singly and doubly excited states, respectively.

The signals are converted to the frequency domain using 2D Fourier transforms with respect to the time differences t_1 and t_3 :

$$\begin{aligned} S^{(I)}(\omega_3, t_2, \omega_1) &= \int_0^\infty \int_0^\infty (S_{GB}^{(I)}(t_3, t_2, t_1) + S_{SE}^{(I)}(t_3, t_2, t_1) + S_{EA}^{(I)}(t_3, t_2, t_1)) \\ &\quad \times \exp(i(\omega_3 t_3 - \omega_1 t_1)) dt_3 dt_1, \\ S^{(II)}(\omega_3, t_2, \omega_1) &= \int_0^\infty \int_0^\infty (S_{GB}^{(II)}(t_3, t_2, t_1) + S_{SE}^{(II)}(t_3, t_2, t_1) + S_{EA}^{(II)}(t_3, t_2, t_1)) \\ &\quad \times \exp(i(\omega_3 t_3 + \omega_1 t_1)) dt_3 dt_1. \end{aligned} \quad (4.14)$$

t_2 is the mixing time. Finally, the 2DIR correlation spectrum is the imaginary part of the sum of the photon-echo and non-rephasing signals,

$$I_{2D}(\omega_3, t_2, \omega_1) = \text{Im}(S^{(I)}(\omega_3, t_2, \omega_1) + S^{(II)}(\omega_3, t_2, \omega_1)). \quad (4.15)$$

The parallel and perpendicular polarization spectra are obtained using the proper orientation averaging over polarization components of the transition dipole vectors as described elsewhere [39, 43].

In Figure 4.1 a flow diagram for the calculation of multi-dimensional spectra is given. The information about the fluctuations in the Hamiltonian and transition-dipoles comes either molecular dynamics simulations or some kind of stochastic model. The parameters connecting the molecular dynamics structures with the actual Hamiltonian can be provided from *ab initio* calculations or some kind of mapping based on such calculations. Finally, the NISE scheme is applied to obtain the spectra.

4.3 Dephasing and lineshapes

The fluctuations affect the shape of the linear spectra. If there is a distribution of frequencies present from different molecules the sum of the signal from all molecules will decay (see Figure 4.2). The time scale for this dephasing is determined by the width of the frequency distribution. For a Gaussian frequency distribution the signal will be given by an oscillation with the central frequency with Gaussian decay. If the frequency of each molecule fluctuates on a time scale faster than the dephasing time each molecule will on average evolve with a frequency that is close to the central frequency and the molecules will all behave in a more similar way

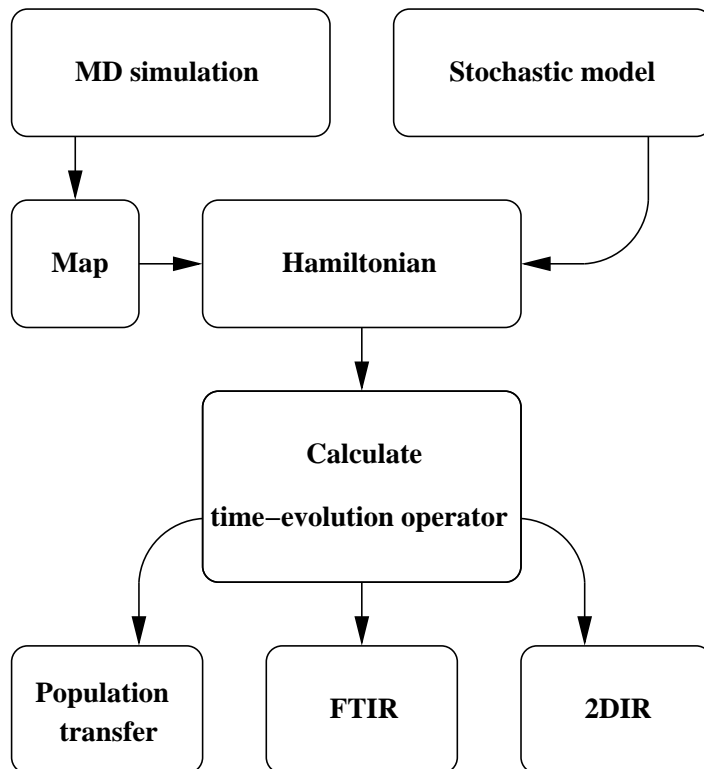


FIGURE 4.1: A flow diagram for the practical calculation of spectra.

resulting in a slowdown of the dephasing. For a Gaussian distribution of frequencies this will lead to an overall signal that oscillates with the central frequency and decay exponentially (see Figure 4.2). These two limiting cases result in Gaussian and Lorentzian line shapes as illustrated in Figure 4.3. The fact that frequency fluctuations make the individual molecules behave more similar with a frequency that is closer to the central frequency leads to narrower lines the faster these fluctuations are. This is also known as motional narrowing. The fluctuations are often characterized by the frequency auto-correlation function.

For two-dimensional IR/vis spectroscopy the frequency fluctuations manifest themselves in a different way. The line shapes are affected by motional narrowing just as for the linear spectra. At the same time the frequency fluctuations can be studied by changing the waiting time. If one excite a molecule during the first time delay and probe it during the third time delay one will observe the signal of that molecule at a point in the spectrum connected with the frequency it had during the first delay along the ω_1 axis and the frequency it had during the third time delay along the ω_3 axis. If the frequency did not change during the waiting time one will therefore observe a diagonally elongated line (see Figure 4.4). If on the other hand the dynamics is very fast compared to the waiting time all molecules will have lost their memory of their initial frequency after the waiting time and the peak will be round (see

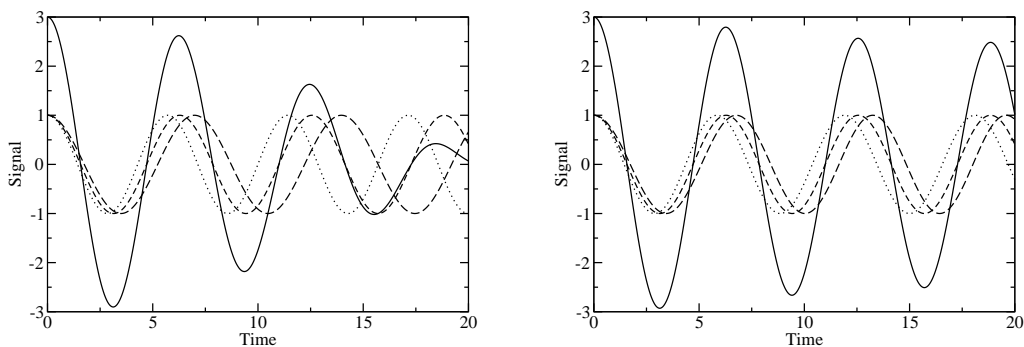


FIGURE 4.2: *Left: The signal from three molecules emitted at different constant frequencies. The total signal dephase rapidly. Right: The signal from three molecules emitted at initially different but rapidly fluctuating frequencies. The total signal dephase slowly.*

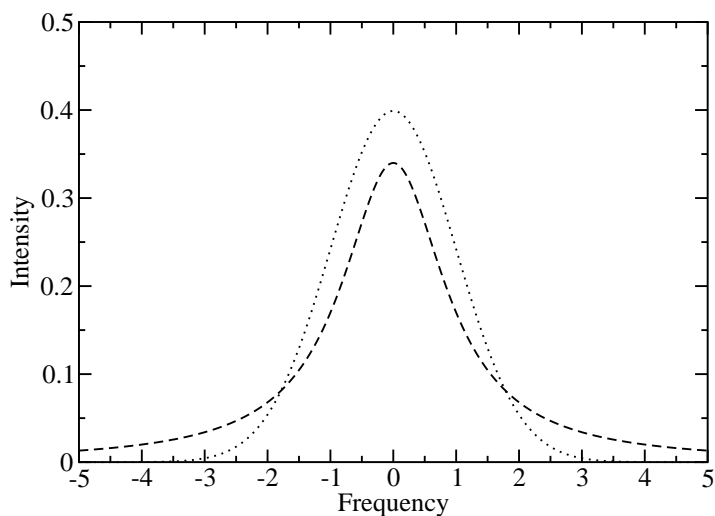


FIGURE 4.3: *The dotted line is a Gaussian lineshape. The dashed line is a Lorentzian lineshape.*

Figure 4.4). At intermediate times the loss of correlation can be followed by looking at the broadening of the peak in the antidiagonal direction or on the slope of the peak. Such studies with varying waiting times are useful in the study of the time scales that the environment around a molecule change, since the frequency fluctuations are induced by this environment.

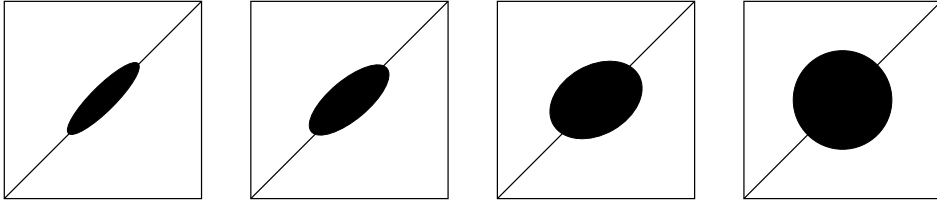


FIGURE 4.4: *The shape of two-dimensional IR/vis spectra. Diagonal elongated lineshapes indicate slow dynamics, while fast dynamics is connected with round lineshapes. As the waiting time increases (from left to right) the frequency memory is lost and the lineshapes get more round.*

4.4 Reorientation

The rotational motion of molecules can be followed using the polarization of laser pulses. When the waiting time is zero the strongest signal will come when all pulses have parallel polarization. If the transition dipole was aligned with the polarization for the first laser pulse it will also be aligned with the polarization for the last laser pulse and therefore the maximal signal is obtained. If the waiting time is increased the molecule and therefore the transition dipole might rotate. The transition dipole is therefore not anymore aligned with the last laser pulse and the signal will decrease (see Figure 4.5). On the other hand, if one uses the perpendicular polarization setup, where polarization of the laser after the waiting time is perpendicular to the laser polarization before, a molecule that was aligned with the laser polarization before the waiting time will need to rotate to be aligned with the laser polarization after the waiting time. Therefore the intensity in the perpendicular polarization setup increase with the rotation of the molecules. Often the isotropic signal is defined as the sum $S_{ISO} = S_{||} + 2S_{\perp}$, where $S_{||}$ is the parallel polarization signal and S_{\perp} is the perpendicular polarization signal. This is sometimes also denoted the magic angle signal, because it can be obtained by rotating the laser polarization after the waiting time by the *magic angle* 54.7° with respect to that before the waiting time. The isotropic signal is independent of the transition-dipole rotation. The transition-dipole rotation is usually characterized by the anisotropy

$$S_{ANI} = \frac{S_{||} - S_{\perp}}{S_{||} + 2S_{\perp}}. \quad (4.16)$$

The anisotropy assuming a fixed transition dipole $\vec{\mu}$ rotating is equal to the rotational correlation function for the unit vector $\hat{\mu}$ along the transition dipole

$$C(t) = \frac{1}{5} \langle 3|\hat{\mu}(t) \cdot \hat{\mu}(0)|^2 - 1 \rangle_E. \quad (4.17)$$

The anisotropy is 0.4, when no rotation has taken place and goes to 0, when an isotropic distribution in three dimensions has been reached. If the rotation is restricted to a plane the

anisotropy will be 0.1, when an isotropic distribution has been obtained within that plane.

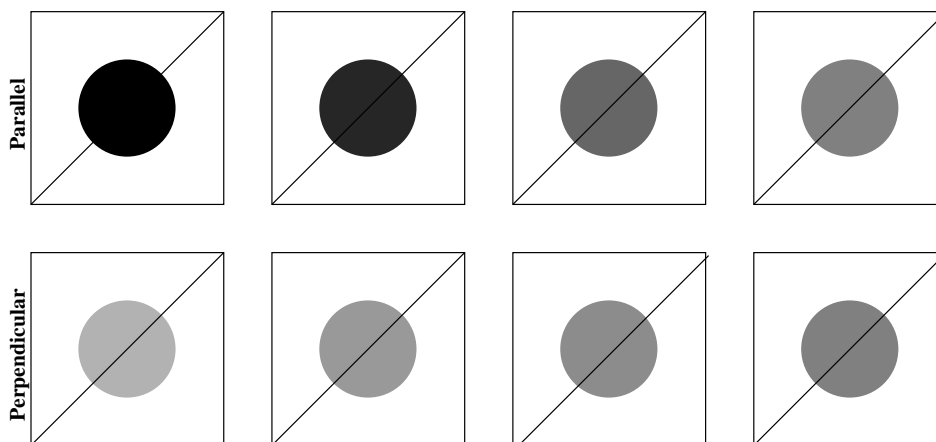


FIGURE 4.5: *The intensity of two-dimensional IR/vis spectra with different polarization. The grayscale indicates the relative intensity to the initial intensity of the parallel polarization spectrum. The top spectra are parallel polarization and the bottom spectra are perpendicular polarization. The waiting time increases from left to right.*

4.5 Population transfer

When the Hamiltonian is fluctuating the normal eigen state picture breaks down. The eigen states at one time are different from the eigen states at another time. Therefore there is a constant mixing of states as the time progresses and if we excited one state the excitation might end up in another state at a later time. This transfer of population leads to effects that are similar to those observed due to dephasing and rotation. When population transfer from one state to another the frequency of that other state can also be different as can the transition dipole. One should therefore be cautious with the interpretation of spectra involving molecules with multiple states that can interact during the waiting time. The population transfer within the single and double excitation manifolds is accounted for with the NISE approach outlined here. One should of course be aware that eventually the population of an excited state will return to the ground state and complex decay through intermediate states is observed experimentally as well. This is only accounted for by the *ad hoc* decay rate of the overall signal. More sophisticated methods still needs to be developed to account properly for those effects.

Bibliography

- [1] T. I. C. Jansen and J. Knoester. *Acc. Chem. Res.*, **42**(9):1405–1411, (2009).
- [2] E. L. Hahn. *Phys. Rev.*, **80**:580, (1950).
- [3] J. B. Udganokar and R. L. Baldwin. *Nature*, **335**:694, (1988).
- [4] H. Roder, G. A. Elove and S. W. Englander. *Nature*, **335**:700, (1988).
- [5] M. Bycroft, A. Matouschek, J. T. Kellis, L. Serrano and A. R. Fersht. *Nature*, **346**:488, (1990).
- [6] R. P. Feynman, F. L. Vernon and R. W. Hellwarth. *J. Appl. Phys.*, **28**:49, (1957).
- [7] N. A. Kurnit, I. D. Abella and R. W. Hartmann. *Phys. Rev. Lett.*, **13**:567, (1964).
- [8] T. W. Mossberg, A. M. Flusberg, R. Kachru and S. R. Hartmann. *Phys. Rev. Lett.*, **42**:1665, (1979).
- [9] K. Duppen, D. P. Weitekamp and D. A. Wiersma. *Chem. Phys. Lett.*, **106**:147, (1984).
- [10] Y. Tanimura and S. Mukamel. *J. Chem. Phys.*, **99**:9496, (1993).
- [11] R. M. Hochstrasser. *Phys. Chem. Comm.*, **3**:U1, (2002).
- [12] P. Hamm, M. H. Lim and R. M. Hochstrasser. *J. Phys. Chem. B*, **102**:6123, (1998).
- [13] S. Woutersen and P. Hamm. *J. Chem. Phys.*, **115**:7737, (2001).
- [14] L. J. Kaufman, J. Heo, L. D. Ziegler and G. R. Fleming. *Phys. Rev. Lett.*, **88**:207402, (2002).
- [15] K. J. Kubarych, C. J. Milne and R. J. D. Miller. *International Reviews in Physical Chemistry*, **22**(3):497–532, (2003).
- [16] T. Brixner, J. Stenger, H. M. Vaswani, M. Cho, R. E. Blankenship and G. R. Fleming. *Nature*, **434**:625, (2005).

BIBLIOGRAPHY

- [17] W. P. de Boeij, M. S. Pshenichnikov and D. A. Wiersma. *Annu. Rev. Phys. Chem.*, **49**:99, (1998).
- [18] S. Mukamel. *Principles of Nonlinear Optical Spectroscopy*. Oxford University Press, New York, 1995.
- [19] R. J. Boyd. *Nonlinear Optics*. Academic Press, San Diego, 1992.
- [20] M. Cho. *Chem. Rev.*, **108**:1331, (2008).
- [21] S. Mukamel. *Annu. Rev. Phys. Chem.*, **51**:691, (2000).
- [22] Y. Tanimura. *J. Phys. Soc. Jp.*, **75**:082001, (2006).
- [23] J. C. Wright. *Int. Rev. Phys. Chem.*, **21**(2):185–255, (2002).
- [24] R. M. Hochstrasser. *P. Nat. Acad. Sci.*, **104**:14190, (2007).
- [25] S. Mukamel, R. Oszwaldowski and L. Yang. *J. Chem. Phys.*, **127**:221105, (2007).
- [26] O. Golonzka, M. Khalil, N. Demirdöven and A. Tokmakoff. *J. Chem. Phys.*, **115**:10814, (2001).
- [27] T. I. C. Jansen, J. G. Snijders and K. Duppen. *J. Chem. Phys.*, **114**:10910, (2001).
- [28] K. Kubarych, C. J. Milne and R. J. D. Miller. *Chem. Phys. Lett.*, **369**:635, (2003).
- [29] D. A. Blank, L. J. Kaufman and G. R. Fleming. *J. Chem. Phys.*, **111**(7):3105, (1999).
- [30] C. J. Milne, Y. L. Li, T. I. C. Jansen, L. Huang and R. J. D. Miller. *J. Phys. Chem. B*, **110**:19867, (2006).
- [31] J. Bredenbeck, A. Ghosh, M. Smits and M. Bonn. *J. Am. Chem. Soc.*, **130**:2152, (2008).
- [32] S. Garrett-Roe and P. Hamm. *J. Chem. Phys.*, **130**:164510, (2009).
- [33] S. Mukamel. *Phys. Rev. A*, **28**:3480, (1983).
- [34] Y. Tanimura and R. Kubo. *J. Phys. Soc. Jp.*, **58**:101, (1989).
- [35] A. Ishizaki and Y. Tanimura. *J. Phys. Chem. A*, **111**:9269, (2007).
- [36] C. J. Fecko, J. D. Eaves, J. J. Loparo, A. Tokmakoff and P. L. Geissler. *Science*, **301**:1698, (2003).
- [37] B. M. Auer and J. L. Skinner. *J. Chem. Phys.*, **128**:224511, (2008).
- [38] J. H. Choi, S. Y. Ham and M. Cho. *J. Phys. Chem. B*, **107**(34):9132–9138, (2003).

BIBLIOGRAPHY

- [39] T. I. C. Jansen and J. Knoester. *J. Chem. Phys.*, **124**:044502, (2006).
- [40] J. Adolphs and T. Renger. *Biophys. J.*, **91**:2778, (2006).
- [41] T. I. C. Jansen and J. Knoester. *J. Phys. Chem. B*, **110**:22910, (2006).
- [42] K. Kwac, H. Lee and M. Cho. *J. Chem. Phys.*, **120**:1477, (2004).
- [43] R. M. Hochstrasser. *Chem. Phys.*, **266**(2-3):273–284, (2001).

BIBLIOGRAPHY
